Nanoscale pattern formation on solid surfaces bombarded by two broad ion beams in the regime in which sputtering is negligible

R. Mark Bradley [ID]

Departments of Physics and Mathematics, Colorado State University, Fort Collins, Colorado 80523, USA

Tejas Sharath

Department of Physics, Colorado State University, Fort Collins, Colorado 80523, USA

We study nanoscale pattern formation on the surface of a solid that is bombarded with two diametrically opposed, broad ion beams for ion energies low enough that sputtering can be neglected. We focus on the case in which the angle of ion incidence is just above the threshold angle for pattern formation. The equation of motion at sufficiently long times is derived using a generalized crater function formalism. This formalism also yields expressions for the coefficients in the equation of motion in terms of crater function moments. We find that virtually defect-free ripples with a sawtooth profile can emerge at sufficiently long times. The ripples also coarsen as time passes, in contrast to the near-threshold behavior of ripples in the higher energy regime in which sputtering is significant.

I. INTRODUCTION

Ion bombardment is a widely employed method of producing nanoscale patterns on solid surfaces [1]. A variety of patterns, which include surface ripples and arrays of nanodots or nanoholes, can be fabricated in a single process step without a mask or photoresist [1–11]. Nanoscale surface ripples in particular will form on virtually any solid target material if the angle of ion incidence, θ, exceeds a critical value θ_c.

Experiments have typically been done with noble gas ions that have energies on the order of 1 keV. In this regime, sputter yields are usually of order unity. For a given target material, ion species, and angle of incidence, the feature size of the nanostructures is found to be an increasing function of the ion energy [1]. To produce smaller feature sizes, therefore, ions of lower energy should be employed.

When the energy of the incident ions is on the order of a few tens of electron volts, sputtering is negligible. Experiments in this low-energy regime are few, but they reveal that nanostructures do form: ripples and disordered arrays of spikes have been observed [12–15]. In addition to its intrinsic scientific interest, the low-energy regime may become important in applications since the feature size of the nanostructures can be below 50 nm.

In the low-energy regime, mass redistribution (MR) takes place: momentum transfer from the incident ions to atoms near the solid surface leads to inelastic displacement of the atoms [16–18]. Depending on the ion energy and target material, dozens of atoms can be displaced even though there is essentially no sputtering. MR is important at ion energies on the order of 1 keV, a regime in which sputter yields are relatively high [19]. It plays an even more crucial role in the low-energy regime in which sputtering is irrelevant [15].

Ions can also be implanted in the low-energy regime. However, when an ion is incident on the solid surface, the result can be at most one implanted ion, whereas, as noted above, dozens of atoms can be displaced. In addition, noble gas ions penetrate only a few nanometers into the solid, are highly mobile, and usually desorb when they reach the solid surface [20]. Implantation of noble gas ions can therefore be neglected [21]. This is confirmed by estimates of the curvature coefficients in the linearized equation of motion obtained using molecular dynamics simulations and the crater function formalism [15].

When sputtering and implantation are neglected, the mass of the solid is conserved. This makes the low-energy limit fundamentally different than the higher energy regime in which sputtering is significant. The equation of motion that is typically adopted in the high-energy regime, the anisotropic Kuramoto-Sivashinsky equation [1,22,23], is not valid in the low-energy regime because it does not conserve mass. In addition, while curvature-dependent sputtering, MR, and ion implantation may all contribute to the surface instability in the higher energy regime, the instability is entirely due to MR in the low-energy regime.

In this paper, we will study the behavior of a solid surface that is bombarded with two low-energy noble gas ion beams with the same angle of incidence, θ, and azimuthal angles that differ by $180°$. We will focus on θ values just above the threshold value θ_c for pattern formation and carry out a systematic expansion in the small parameter $\epsilon \equiv (\theta - \theta_c)^{1/2}$. It will be shown that the equation of motion (EOM) has the form

$$u_t = au_{xx} + Du_{yy} - Bu_{xxxx} + c\partial_x u_x^3 + \beta\partial_x^2 u_x^2 \qquad (1)$$

for sufficiently low ion fluxes. Here $u(x, y, t)$ is the height of the surface above the point (x, y) in the x-y plane at time t

and the subscripts x, y, and t on u denote partial derivatives. In Eq. (1), D and B are positive, c and β are non-negative, and a changes sign from positive to negative as θ is increased through θ_c. Simulations of the EOM (1) show that dual-beam ion bombardment can lead to the formation of ripples with a high degree of order, a finding that may prove to be quite useful in applications. The ripples also coarsen; i.e., their wavelength and amplitude increase with time. In contrast, in the higher energy regime in which significant sputtering occurs, the ripples that form in the dual-beam problem with θ just above θ_c are disordered and do not coarsen [24].

In our derivation of the EOM (1), we will utilize a generalized crater function formalism (CFF). The crater function is the average result of many ion impacts at a particular surface point, and so is effectively the Green's function for the problem. The CFF allows us to determine the response of a surface to bombardment with a broad ion beam if the crater function is known [24–26]. This approach takes into account the effect of ion-induced mass redistribution but does not rely on the simple, approximate model of this phenomenon introduced by Carter and Vishnykov [16]. Our CFF yields explicit expressions for the coefficients a, D, B, c, and β that appear in the EOM (1). These expressions relate the coefficients to moments of the crater function, and so could be used to estimate the coefficients using input from atomistic simulations.

In Ref. [24], a generalized CFF was developed for the regime in which the ion energy is high enough that sputtering is significant. That generalized CFF was used to derive the EOM that applies for incidence angles just above the threshold angle for pattern formation θ_c. In this paper, we will employ an analogous CFF to derive the EOM that applies for θ just above θ_c in the low-energy regime in which sputtering is negligible. Although there are parallels between high- and low-energy regimes, there are important differences in the CFFs for the two problems, and the equations of motion are fundamentally different.

As we will see, the problem in which diametrically opposed beams are simultaneously incident on the solid surface is much simpler than the problem in which there is a single incident beam. In an experiment, two ion beams would probably not be used. Instead, the sample would likely be rotated periodically through 180° increments about its normal while being bombarded with a single obliquely incident beam. If the time between rotations were made sufficiently small, the effect would be essentially the same as if the sample were concurrently bombarded with diametrically opposed beams.

Experiments with dual ion beams have been carried out in the past, but the azimuthal angles of the beams differed by 90° rather than 180° [27,28]. In addition, the sample has been rotated once through a 90° azimuthal angle during bombardment with a single obliquely incident ion beam [28,29]. The effect of repeated rotations through an azimuthal angle of 180° has been studied theoretically for binary target materials, but only in the early-time linear regime [30]. In all of these studies, the ion energies were high enough that sputtering had an important effect [31].

This paper is organized as follows. After making some introductory remarks in Sec. II, we introduce the crater function that we will employ in Sec. III. In Sec. IV, we develop our

generalized crater function formalism and derive the EOM for the case in which a single beam is incident on the sample surface. The EOM for the case in which diametrically opposed beams are incident on the surface is derived, analyzed, and discussed in Sec. V. Problematic aspects of the single-beam EOM are the subject of Sec. VI. We discuss our results in Sec. VII and conclude in Sec. VIII.

II. PRELIMINARY CONSIDERATIONS

We will begin by considering the bombardment of a solid elemental material with a single broad beam of noble gas ions before moving on to the case in which two diametrically opposed beams are incident on the surface. The material may be amorphous or crystalline. If the material is initially crystalline, we assume that a layer at the surface of the solid is amorphized by the ion bombardment. As stated in the Introduction, we will make the customary assumption that the effect of ion implantation is negligible [21]. Finally, we will take the sample temperature to be low enough that the effect of thermally activated surface diffusion is negligible compared to the effect of ion-induced surface viscous flow [32].

The sample surface will be taken to be nominally flat before the irradiation begins. The unit vector $\hat{z}$ will be chosen to be normal to the macroscopic surface and to point away from the solid. We define the unit vector $\hat{x}$ to lie in the direction of the projection of the incident ion beam onto the macroscopic surface. The incident ion flux is $\boldsymbol{J} = -J\hat{e}$, where $\hat{e} \equiv -\hat{x} \sin\theta + \hat{z} \cos\theta$ and the angle of incidence, θ, is the angle between the global vertical and the incident beam.

We assume that the surface remains flat for $\theta < \theta_c$ and that parallel-mode ripples develop for $\theta > \theta_c$. A morphological transition of this kind has been observed in single-beam experiments in the low-energy regime [12,15].

We will employ a continuum description of the surface dynamics in which the position of an arbitrary point on the surface is given by $\boldsymbol{r} = x\hat{x} + y\hat{y} + u(x, y, t)\hat{z}$, where $u(x, y, t)$ is the height of the point above the x-y plane at time t. The surface height u is obtained by coarse-graining the detailed microscopic surface configuration and is assumed to be a smoothly varying function of its arguments x, y, and t.

III. THE CRATER FUNCTION

The crater function describes the average effect of a single ion impact on the morphology of the solid surface. The crater function that we will employ was first introduced in Ref. [24]. In this section, we will find it convenient to place the origin O at the point of ion impact.

The value of the crater function f at the point (x, y) is defined to be minus the average change in the surface height u above the point (x, y) in the x-y plane as a result of a single ion impact at $x = y = 0$ [24,26]. The crater function f depends on x, y and the angle of incidence, θ. It also depends on the shape of the entire surface, or, equivalently, on all of the spatial derivatives of $u(x, y, t)$ evaluated at $x = y = 0$. We will write

$$f = f(x, y, \theta; u_x, u_y, u_{xx}, u_{xy}, u_{yy}, u_{xxx},$$
$$u_{xxy}, u_{xyy}, u_{yyy}, u_{xxxx}, \ldots). \tag{2}$$

The partial derivatives of u that appear on the right-hand side of Eq. (2) are all to be evaluated at $x = y = 0$. We assume that f is known *a priori* from another theory or from atomistic simulations. Because the mass of the solid is conserved,

$$\int f(x, y, \theta; u_x, u_y, u_{xx}, u_{xy}, u_{yy}, u_{xxx}, \ldots) d^2 x = 0, \quad (3)$$

where $d^2 x \equiv dx\, dy$.

We will take the crater function f to be evaluated at a time long enough after the ion impact that nearly all ion-induced motion has ceased. It therefore takes into account mass redistribution and ion-induced surface viscous flow. When a broad beam is incident on the surface, we will assume that the ion flux is low enough that essentially all ion-induced motion near a point of impact, **P**, has ended before another ion strikes the surface in the vicinity of **P**.

IV. SINGLE-BEAM EQUATION OF MOTION

We will begin this section by finding u_t at an arbitrary point $\mathbf{P}_0$ on the solid surface for all times $t \geqslant 0$. The case in which a single broad beam of noble gas ions is incident on the solid will be considered. We will now find it convenient to place the origin O at the position of $\mathbf{P}_0$ at time t. The origin will be taken to be stationary, and so it will remain fixed as the surface point $\mathbf{P}_0$ moves either up or down.

The flux of ions through a surface element dA centered on $\mathbf{r}$ is $J\hat{e} \cdot \hat{n} dA$, where the surface normal $\hat{n}$ is given by

$$\hat{n} = \frac{\hat{z} - \nabla u}{\sqrt{1 + (\nabla u)^2}} \quad (4)$$

and $dA = \sqrt{1 + (\nabla h)^2}\, dx\, dy$. Each arriving ion produces a crater which changes the height of the surface point $\mathbf{P}_0$. It follows that the value of u_t at $x = y = 0$ is given by

$$u_t = -J \int dx \int dy f(-x, -y, \theta; u_x, u_y, u_{xx}, u_{xy}, u_{yy}, \ldots)$$
$$\times (\cos\theta + u_x \sin\theta). \quad (5)$$

All of the spatial derivatives of u that appear in the integrand on the right-hand side of Eq. (5) are evaluated at the point (x, y) in the x-y plane.

Equation (5) completely specifies the dynamics of the surface but it is an exceedingly complicated integro-differential equation. It becomes much simpler when $\epsilon \equiv (\theta - \theta_c)^{1/2}$ is small and positive, however. We seek solutions to Eq. (5) of the form

$$u(x, y, t) = U(X, Y, T), \quad (6)$$

where

$$X \equiv \epsilon x, \quad Y \equiv \epsilon^2 y, \quad \text{and} \quad T \equiv \epsilon^4 t. \quad (7)$$

X, Y, and T are the so-called "slow" variables and x, y, and t are the corresponding "fast" variables. Heuristically speaking, Eqs. (6) and (7) say that for θ close to the critical angle θ_c, the height of the surface disturbance varies slowly in space and time. In addition, the spatial variation in the y direction is more gradual than in the x direction because parallel-mode ripples develop for $\theta > \theta_c$. An *a posteriori* justification for adopting the scaling ansatz given by Eqs. (6) and (7) will be

obtained once we have arrived at an EOM that is well behaved in the $\epsilon \to 0$ limit for the case in which diametrically opposed beams are incident on the target's surface. The scaling given by Eqs. (6) and (7) differs from the scaling that applies when the ion energy is high enough that sputtering is appreciable [24].

The crater function f depends on the fast spatial variables x and y since it varies over distances on the order of the characteristic size of a collision cascade a_0. It is also a function of the slow spatial variables X and Y because it depends on the spatial derivatives of u. These derivatives vary only over distances comparable to the ripple wavelength l, and l is much larger than a_0 close to threshold.

Applying Eqs. (6) and (7), Eq. (5) becomes

$$\epsilon^4 U_T = -J \int dx \int dy f(-x, -y, \theta; \epsilon U_X, \epsilon^2 U_Y,$$
$$\epsilon^2 U_{XX}, \epsilon^3 U_{XY}, \ldots)(\cos\theta + \epsilon U_X \sin\theta). \quad (8)$$

On the left-hand side of Eq. (8), $U_T = U_T(0, 0, T)$. All of the spatial derivatives of U that appear on the right-hand side of Eq. (8) have the arguments X, Y, and T.

We now expand the right-hand side of Eq. (8) in powers of ϵ and retain terms up to fourth order in ϵ. This results in an equation too lengthy to reproduce here. Our next step is to carry out a Taylor series expansion of $U(X, Y, T)$ about the point $X = Y = 0$: we set

$$U(X, Y, T) = \sum_{n=0}^{\infty} \sum_{m=0}^{\infty} S_{n,m}(T) \frac{X^n Y^m}{n!\, m!}, \quad (9)$$

where

$$S_{n,m}(T) \equiv \frac{\partial^{n+m} U}{\partial X^n \partial Y^m}(0, 0, T). \quad (10)$$

We also introduce new dummy variables of integration, $\tilde{x} = -x$ and $\tilde{y} = -y$, and then drop the tildes. In this part of the calculation, we again retain terms up to fourth order in ϵ. So that we can write down the resulting equation succinctly, we define

$$f_0(x, y, \theta) \equiv f(x, y, \theta; 0, 0, \ldots), \quad (11)$$

$$f_1(x, y, \theta) \equiv \frac{\partial}{\partial u_x} f(x, y, \theta; u_x, 0, 0, \ldots)|_{u_x=0}, \quad (12)$$

$$f_2(x, y, \theta) \equiv \frac{\partial}{\partial u_y} f(x, y, \theta; 0, u_y, 0, 0, \ldots)|_{u_y=0}, \quad (13)$$

$$f_3(x, y, \theta) \equiv \frac{\partial}{\partial u_{xx}} f(x, y, \theta; 0, 0, u_{xx}, 0, 0, \ldots)|_{u_{xx}=0}, \quad (14)$$

and so on. Similarly, for positive integers i and j, $f_{i,j}(x, y, \theta)$ will denote the partial derivative of $f(x, y, \theta; u_x, u_y, u_{xx}, u_{xy}, \ldots)$ with respect to the ith and jth arguments that appear after the semicolon, evaluated for all the arguments after the semicolon set equal to zero. For example,

$$f_{1,3}(x, y, \theta) \equiv \frac{\partial}{\partial u_x} \frac{\partial}{\partial u_{xx}} f(x, y, \theta; u_x, 0, u_{xx}, 0, 0, \ldots)|_{u_x=u_{xx}=0}. \quad (15)$$

In addition, we define the crater function moments

$$M^{n,m} \equiv \iint x^n y^m f_0(x, y, \theta) dx dy, \tag{16}$$

$$M_i^{n,m} \equiv \iint x^n y^m f_i(x, y, \theta) dx dy, \tag{17}$$

$$M_{i,j}^{n,m} \equiv \iint x^n y^m f_{i,j}(x, y, \theta) dx dy, \tag{18}$$

and so forth, where n and m are non-negative integers and i and j are positive integers. It is important to note that since mass is conserved,

$$M^{0,0} = M_i^{0,0} = M_{i,j}^{0,0} = M_{i,j,k}^{0,0} = 0 \tag{19}$$

for all positive integers i, j, and k. Equation (19) yields a very significant simplification in the final result of the calculation, which is

$$J^{-1}\epsilon^4 U_T = \epsilon^2 C_{11} S_{2,0} + \epsilon^3 C_{111} S_{3,0} + \epsilon^4 C_{1111} S_{4,0} + \epsilon^4 C_{22} S_{0,2}$$
$$+ 2\epsilon^4 \rho \left(S_{1,0} S_{3,0} + S_{2,0}^2 \right) + 2\epsilon^3 \gamma_2 S_{1,0} S_{2,0}$$
$$+ 3\epsilon^4 \gamma_3 S_{1,0}^2 S_{2,0}. \tag{20}$$

Here

$$C_{11} = M_1^{1,0} \cos\theta + M^{1,0} \sin\theta, \tag{21}$$

$$C_{111} = \left(-\tfrac{1}{2} M_1^{2,0} + M_3^{1,0} \right) \cos\theta - \tfrac{1}{2} M^{2,0} \sin\theta, \tag{22}$$

$$C_{1111} = \left(\tfrac{1}{6} M_1^{3,0} - \tfrac{1}{2} M_3^{2,0} + M_6^{1,0} \right) \cos\theta + \tfrac{1}{6} M^{3,0} \sin\theta, \tag{23}$$

$$C_{22} = M_2^{0,1} \cos\theta, \tag{24}$$

$$\rho = \tfrac{1}{4} \left(2 M_{1,3}^{1,0} - M_{1,1}^{2,0} \right) \cos\theta + \left(M_3^{1,0} - M_1^{2,0} \right) \sin\theta, \tag{25}$$

$$\gamma_2 = \tfrac{1}{2} M_{1,1}^{1,0} \cos\theta + M_1^{1,0} \sin\theta, \tag{26}$$

and

$$\gamma_3 = \tfrac{1}{6} M_{1,1,1}^{1,0} \cos\theta + \tfrac{1}{2} M_{1,1}^{1,0} \sin\theta. \tag{27}$$

Recalling the definition of $S_{n,m}$ [Eq. (10)], Eq. (20) becomes

$$J^{-1} U_T = \epsilon^{-2} C_{11} U_{XX} + \epsilon^{-1} C_{111} U_{XXX} + C_{1111} U_{XXXX}$$
$$+ C_{22} U_{YY} + \rho \partial_X^2 U_X^2 + \epsilon^{-1} \gamma_2 \partial_X U_X^2 + \gamma_3 \partial_X U_X^3, \tag{28}$$

where all of the partial derivatives of U are evaluated at $X = Y = 0$. Equation (28) holds for $X = Y = 0$. However, because we placed the origin at an arbitrary surface point, this partial differential equation is actually valid for all X and Y. Equation (28) is invariant under the transformation $Y \to -Y$, as it must be.

The EOM (28) becomes

$$J^{-1} u_t = C_{11} u_{xx} + C_{22} u_{yy} + C_{111} u_{xxx} + C_{1111} u_{xxxx}$$
$$+ \rho \partial_x^2 u_x^2 + \gamma_2 \partial_x u_x^2 + \gamma_3 \partial_x u_x^3 \tag{29}$$

when written in terms of the original, unscaled variables. The coefficients on the right-hand side of Eq. (29) depend on the

angle of incidence, θ, and are related to the crater function moments by Eqs. (21)–(27). The expressions for C_{11}, C_{22}, C_{111}, and C_{1111} derived in Ref. [24] reduce to our results (21)–(24) for the case in which mass is conserved.

Equation (29) can be written in the form

$$u_t = -\Omega(\partial_x j_x + \partial_y j_y), \tag{30}$$

where Ω is the atomic volume and the surface atomic current $\boldsymbol{j} = j_x \hat{\boldsymbol{x}} + j_y \hat{\boldsymbol{y}} + j_z \hat{\boldsymbol{z}}$ is everywhere tangent to the solid surface. The components j_x and j_y of the surface current are given by

$$j_x = -\Omega^{-1} J \left(C_{11} u_x + C_{111} u_{xx} + C_{1111} u_{xxx} \right.$$
$$\left. + 2\rho u_x u_{xx} + \gamma_2 u_x^2 + \gamma_3 u_x^3 \right) \tag{31}$$

and

$$j_y = -\Omega^{-1} J C_{22} u_y, \tag{32}$$

respectively. Equation (30) shows explicitly that the mass of the solid is a conserved quantity.

In the Carter-Vishnyakov (CV) model of mass redistribution, the magnitude of the surface current j depends only on the local angle of incidence, or, equivalently, on θ, u_x, and u_y [16]. It may therefore seem surprising that in general j_x depends on u_{xx}. Molecular dynamics simulations of ion impacts on a sinusoidally rippled surface show that the mass current is larger at the base of a trough than at the top of a crest, however [20]. These simulations therefore strongly suggest that j_x does indeed depend on u_{xx}. It is this dependence that leads to the presence of the linearly dispersive term $C_{111} u_{xxx}$ and of the so-called conserved Kuramoto-Sivashinsky (CKS) nonlinearity $\rho \partial_x^2 u_x^2$ in the EOM (29).

V. SURFACE DYNAMICS WITH DIAMETRICALLY OPPOSED BEAMS

A. Derivation of the equation of motion

We now turn our attention to the problem in which there are two diametrically opposed beams, each with ion flux $J/2$. (Recall that the beams have the same polar angle but their azimuthal angles differ by $180°$.) If only the beam that is incident from the left were present, the EOM would be Eq. (28) with J replaced by $J/2$:

$$U_T = \frac{J}{2} \left(\epsilon^{-2} C_{11} U_{XX} + \epsilon^{-1} C_{111} U_{XXX} + C_{1111} U_{XXXX} \right.$$
$$\left. + C_{22} U_{YY} + \rho \partial_X^2 U_X^2 + \epsilon^{-1} \gamma_2 \partial_X U_X^2 + \gamma_3 \partial_X U_X^3 \right). \tag{33}$$

Conversely, if only the beam that is incident from the right were present, the EOM would be Eq. (33) with X replaced by $-X$:

$$U_T = \frac{J}{2} \left(\epsilon^{-2} C_{11} U_{XX} - \epsilon^{-1} C_{111} U_{XXX} + C_{1111} U_{XXXX} \right.$$
$$\left. + C_{22} U_{YY} + \rho \partial_X^2 U_X^2 - \epsilon^{-1} \gamma_2 \partial_X U_X^2 + \gamma_3 \partial_X U_X^3 \right). \tag{34}$$

To get U_T when both beams are turned on, we take the sum of the right-hand sides of Eqs. (33) and (34) to yield

$$U_T = J \left(\epsilon^{-2} C_{11} U_{XX} + C_{1111} U_{XXXX} + C_{22} U_{YY} \right.$$
$$\left. + \rho \partial_X^2 U_X^2 + \gamma_3 \partial_X U_X^3 \right). \tag{35}$$

Note that in addition to being invariant under the transformation $Y \to -Y$, the dual-beam EOM (35) is invariant under

$X \to -X$, as it must be. Equation (35) holds for θ just above the critical angle θ_c, i.e., for small $\epsilon = (\theta - \theta_c)^{1/2}$.

Experiments carried out with a single incident ion beam show that parallel-mode ripples form for θ greater than the critical angle θ_c and that the surface remains flat for $\theta < \theta_c$: see Refs. [12,15]. We assume that this remains true in the problem with diametrically opposed beams. For solutions to Eq. (35) to be in agreement with this assumption, C_{11} must be positive for $\theta < \theta_c$, zero for $\theta = \theta_c$, and negative for $\theta > \theta_c$. Carrying out a Taylor series expansion of $C_{11} = C_{11}(\theta)$ about the point $\theta = \theta_c$ yields $C_{11} = -A_{11}(\theta - \theta_c) + O((\theta - \theta_c)^2)$, where the constant A_{11} is non-negative. We neglect the correction term of order $(\theta - \theta_c)^2$ and so obtain $C_{11} \cong -A_{11}\epsilon^2$. We will assume that A_{11} is nonzero.

If C_{22} were negative for $\theta = \theta_c$, it would also be negative for θ slightly less than θ_c. Since C_{11} is positive for θ slightly less than θ_c, perpendicular-mode ripples would develop for θ just below θ_c. Because this is not observed in single-beam experiments, we assume that C_{22} is non-negative for $\theta = \theta_c$. We exclude the anomalous special case in which $C_{22}(\theta_c)$ is zero so that $C_{22}(\theta_c)$ is positive.

Equation (35) may now be written

$$J^{-1}U_T = -A_{11}U_{XX} + C_{1111}U_{XXXX} + C_{22}U_{YY} + \rho\partial_X^2 U_X^2 + \gamma_3\partial_X U_X^3. \quad (36)$$

Notice that ϵ does not appear in Eq. (36). Thus, the scaling we posited in Eqs. (6) and (7) leads to a well-behaved EOM in the small-ϵ limit. Moreover, all of the terms are of the same order in ϵ.

The EOM (35) becomes

$$J^{-1}u_t = C_{11}u_{xx} + C_{22}u_{yy} + C_{1111}u_{xxxx} + \rho\partial_x^2 u_x^2 + \gamma_3\partial_x u_x^3 \quad (37)$$

when written in terms of the unscaled variables. If C_{1111} were positive or zero, arbitrarily short wavelengths would be linearly unstable and the continuum description would break down. We therefore assume that $C_{1111} < 0$. In addition, γ_3 cannot be negative since if it were, the slope of the surface would grow without bound. To simplify the notation, we set $a = JC_{11}$, $D = JC_{22}$, $B = -JC_{1111}$, $c = J\gamma_3$, and $\beta = J\rho$, where $D > 0$, $B > 0$, and $c \geqslant 0$ are constants. Equation (37) is then identical to Eq. (1). By replacing u by $-u$ if necessary, we can also arrange for β to be non-negative.

The term $c\partial_x u_x^3$ in Eq. (1) is familiar from the theory of the mounding instability that can occur during molecular beam epitaxy. There the term results from the Ehrlich-Schwoebel (ES) effect and can lead to the formation of a faceted surface [33]. In our problem, the slope dependence of the surface current produced by MR leads to the presence of this term. The term $\beta\partial_x^2 u_x^2$, on the other hand, is the CKS nonlinearity. Although this term was first encountered in molecular beam epitaxy [33,34], it is believed to play a role in ion-induced pattern formation even when a surface layer of the target material is amorphized by the ion bombardment [35–37]. The CKS nonlinearity tends to produce coarsening of the surface patterns, i.e., the characteristic lateral and vertical length scales increase with time. It also breaks the $u \to -u$ symmetry that would be present if β were zero. Since there is vacuum above the surface and solid below, there is no reason that such a symmetry should exist.

B. Analysis of the equation of motion

Because the surface of the solid is nominally flat initially, Eq. (1) can be linearized at early times. The amplitude of a sinusoidal ripple with wave vector $\boldsymbol{k} = k_x\hat{\boldsymbol{x}} + k_y\hat{\boldsymbol{y}}$ increases exponentially in time with the rate

$$\sigma(\boldsymbol{k}) = -ak_x^2 - Dk_y^2 - Bk_x^4. \quad (38)$$

[The ripple amplitude decays exponentially if $\sigma(\boldsymbol{k})$ is negative.] It follows that for $a < 0$, ripples with wave number $\sqrt{|a|/(2B)}$ and with their wave vector along the x direction emerge shortly after the irradiation begins. Conversely, the surface becomes flatter if $a > 0$.

Consider the case $a < 0$, so that a flat initial surface is unstable and pattern formation occurs. If u is independent of y, Eq. (1) reduces to a partial differential equation (PDE) in one dimension. For $\beta = 0$, we set $\phi \equiv u_x$. Differentiating the one-dimensional (1D) PDE with respect to x yields

$$\phi_t = a\phi_{xx} - B\phi_{xxxx} + c\partial_x^2\phi^3, \quad (39)$$

which is the 1D Cahn-Hilliard (CH) equation [38]. This leads us to the conclusion that for long times the solution to the 1D PDE with $\beta = 0$ tends to a state in which most of the surface has a slope nearly equal to one of the two selected values $\pm(|a|/c)^{1/2}$. The slope changes rapidly in interfacial regions between adjacent intervals with nearly constant slope. As some regions of nearly constant slope contract and then disappear and others expand, the pattern coarsens. For $c = 0$, on the other hand, the 1D PDE is the CKS equation, which has been studied as a model of amorphous thin film growth [39] and the step meandering instability on a crystal surface [40]. A family of periodic steady-state solutions to the CKS equation exists [39]; these consist of concave, nearly parabolic segments that meet at "kinks." These kinks are not discontinuities in u_x, but are instead relatively narrow regions where u_{xx} is negative. For generic nominally flat initial conditions, a nearly periodic pattern with the linearly selected wave number emerges at early times, but at longer times coarsening occurs: kinks merge and the average size of the parabolic segments grows in time [40].

Before proceeding further, we will recast the full two-dimensional EOM (1) that applies when u is not independent of y in dimensionless form to reduce the number of parameters to a minimum. We introduce the dimensionless quantities

$$\tilde{x} \equiv \left(\frac{|a|}{B}\right)^{1/2}x, \quad \tilde{y} \equiv \frac{|a|}{(DB)^{1/2}}y, \quad \tilde{t} \equiv \frac{|a|^2}{B}t, \quad \text{and}$$

$$\tilde{u} = \frac{\sqrt{\beta^2 + Bc}}{B}u. \quad (40)$$

We will also drop the tildes for the remainder of this subsection. Equation (1) becomes

$$u_t = -u_{xx} - u_{xxxx} + u_{yy} + (\cos^2\psi)\partial_x u_x^3 + (\sin\psi)\partial_x^2 u_x^2, \quad (41)$$

where the angle $\psi \in [0, \pi/2]$ is defined by the relation $\tan\psi = \beta/\sqrt{Bc}$. For $\psi = 0$, we differentiate Eq. (41) with respect to x and so obtain

$$\phi_t = -\phi_{xx} - \phi_{xxxx} + \phi_{yy} + \partial_x^2\phi^3. \quad (42)$$

Equation (42) is an anisotropic generalization of the 1D CH equation to two dimensions. On the other hand, for $\psi = \pi/2$ (or, equivalently, for $c = 0$), Eq. (41) is an anisotropic generalization of the 1D CKS equation to two dimensions. Equation (41) depends on the single dimensionless parameter ψ that measures the relative strength of the quadratic and cubic nonlinearities.

Let us consider the behavior of solutions to Eq. (41) with $\psi = 0$ on the domain in which $0 \leqslant x \leqslant L$ and $0 \leqslant y \leqslant L$ and apply periodic boundary conditions. We introduce the effective free energy

$$\mathcal{F} \equiv \int_0^L \int_0^L \left[\frac{1}{2} u_{xx}^2 + v(u_x, u_y) \right] dx\, dy, \qquad (43)$$

where

$$v(u_x, u_y) \equiv \frac{1}{4} \left(u_x^2 - 1 \right)^2 + \frac{1}{2} u_y^2 \qquad (44)$$

will be referred to as the effective potential. Equation (41) can be written

$$u_t = -\frac{\delta \mathcal{F}}{\delta u}, \qquad (45)$$

where $\delta \mathcal{F}/\delta u$ denotes the variational derivative of $\mathcal{F}$ with respect to the surface height u. Equation (45) implies that $d\mathcal{F}/dt \leqslant 0$, i.e., the effective free energy can never increase. The dynamics therefore tends to minimize the value of $\mathcal{F}$. The effective potential v has minima at $(u_x, u_y) = (\pm 1, 0)$. Therefore, the surface will tend toward a state in which most of the surface has a gradient ∇u nearly equal to $\pm \hat{x}$; i.e., the surface will facet. A flat facet with one of the two selected gradients $\pm \hat{x}$ has a free energy equal to zero. Adjacent facets are separated by "edges" which have a positive free energy per unit length. ∇u changes rapidly but not discontinuously as an edge is traversed.

Figures 1(a)–1(c) show the results of a simulation of Eq. (41) with $\psi = 0$ and a low-amplitude spatial white noise initial condition. (For details of the method of numerical integration we employed, see Ref. [41].) At early times, the ripple wavelength is close to the linearly selected wavelength and there is no selected slope. The ripple pattern becomes progressively more faceted as time passes. The dislocations present in the ripple pattern climb (i.e., move roughly parallel to the y axis) until they meet dislocations of opposite sign and annihilate one another. In this way, the average width of the facets grows and the total length of the edges decreases, leading to a reduction in the effective free energy of the surface. As expected, the slope distribution has two pronounced peaks at $(u_x, u_y) = (\pm 1, 0)$ at long times, as shown in Fig. 2(a) for $t = 5000$. All of the dislocations have disappeared at this point and the time evolution has become very slow. However, although dislocations are no longer present, the wavelength of the pattern varies as we move along the x direction [see Fig. 2(d)]. The order is not perfect as a consequence.

Even though Eq. (41) cannot be written in the variational form (45) for $0 < \sin \psi \leqslant 1$, the behavior we find for $\sin \psi = 0.2, 0.5, 0.7$, and 0.9 is qualitatively similar to what we observed for $\sin \psi = 0$. Figures 1(d)–1(f) show the time evolution of the surface for $\sin \psi = 0.9$, for example. As for $\sin \psi = 0$, the pattern coarsens with time and all of the dislocations eventually mutually annihilate. There are also sharp

peaks in the slope distribution, but the selected slope is larger than for $\sin \psi = 0$. This is illustrated by Fig. 2(b) for the case $\sin \psi = 0.9$.

For $\sin \psi = 1$, ripples with their average wave vector oriented in the x direction emerge and coarsen in time, just as for $\sin \psi < 1$: see Figs. 1(g)–1(i) [42]. Once again, no dislocations are present in the pattern at sufficiently long times. However, the ripples that develop for $\sin \psi = 1$ are not faceted, as Fig. 2(c) illustrates. This is because the ES term is responsible for the formation of facets and it is not present in the EOM for $\sin \psi = 1$.

Whatever the value of $\sin \psi$, there are no dislocations present in the ripple pattern at sufficiently long times. However, as the cuts through the surface shown in Figs. 2(d)–2(f) show, the wavelength varies with x and the surface is not perfectly ordered. This is to be expected, because the band of linearly unstable wavelengths is not narrow.

As we have seen, the mean wavelength of the ripples Λ and the interface width increase as time passes. A natural question to ask is whether these quantities exhibit power-law scaling. We adopted the root-mean-square deviation of the surface height from its mean value w as a measure of the interface width. In our simulations, we found that w grows exponentially at early times, as one would expect (not shown). The value of w then quickly saturates or enters a regime of very slow growth—our numerical results do not permit us to determine which of these behaviors actually occurs. We also find that Λ is comparable to the linearly selected wavelength at early times. At later times, it grows but then appears to saturate. In both cases, we do not observe scaling behavior between the early-time and long-time behavior. The fluctuations are also large, which would necessitate averaging over many simulations to obtain results with an acceptable degree of accuracy.

We can gain some insight into this situation in the following way. The anisotropic CH equation obtained for $\psi = 0$ [Eq. (42)] is smoothing in the y direction. Its behavior is therefore somewhat similar to that of the 1D CH equation. The coarsening of the 1D CH equation is very slow (it is logarithmic [43]) and is therefore not easily studied numerically. We believe that the same type of very slow coarsening occurs in our two-dimensional (2D) EOM (41) for $\psi < \pi/2$.

C. The existence of selected slopes for diametrically opposed beams

As we have seen, if θ is just above the critical angle θ_c and $c > 0$, the surface evolves a state in which there are large regions with slope very nearly equal to one of the two selected values. The goal of this subsection is to provide some physical insight into how there can be nonzero selected slopes when diametrically opposed beams are incident on the solid surface. To make this discussion as transparent as possible, we will take the surface height u to be independent of y.

Consider the surface current j when a single ion beam is incident on the solid. For the sake of simplicity, we assume that j depends only on the local angle of incidence, θ_{loc}, as in the CV model. In general, $j(\theta_{\mathrm{loc}})$ must be an odd function of θ_{loc} and must vanish for θ_{loc} equal to 0 and $\pi/2$. In addition, $j(\theta_{\mathrm{loc}})$ must be positive for $0 < \theta_{\mathrm{loc}} < \pi/2$ since the current points
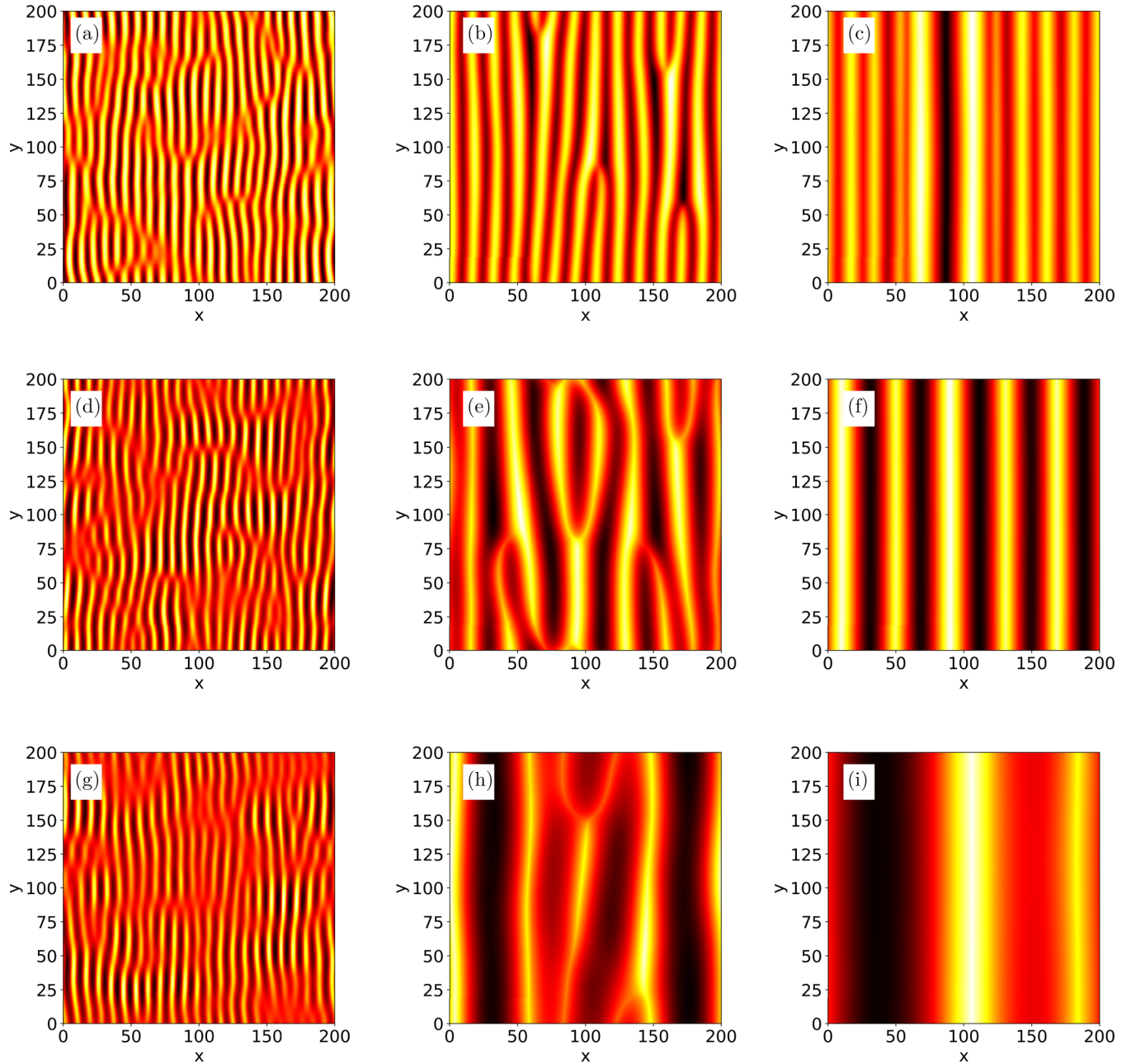
FIG. 1. Top: Simulation of Eq. (41) with $\sin \psi = 0$ at (a) $t = 50$, (b) $t = 1000$, and (c) $t = 5000$. Middle: Simulation with $\sin \psi = 0.9$ at (d) $t = 50$, (e) $t = 1000$, and (f) $t = 5000$. Bottom: Simulation with $\sin \psi = 1$ at (a) $t = 50$, (b) $t = 1000$, and (c) $t = 5000$. The domain size was 200×200 in all three simulations.

in the projected beam direction. In the case of the CV model, $j(\theta_{\text{loc}}) = \mu J \cos \theta_{\text{loc}} \sin \theta_{\text{loc}}$, where μ is a positive constant of proportionality. This current satisfies all of the requirements we have listed, but is unlikely to be exactly correct for any beam-target combination.

Let $\alpha \equiv \tan^{-1} u_x$ be the angle that the surface is tilted away from the horizontal. The total current when two diametrically opposed beams are incident on the surface is $j_{\text{tot}} = [j(\theta - \alpha) - j(\theta + \alpha)]/2$. For the CV model,

$$j_{\text{tot}} = -\frac{1}{2} \mu J \cos(2\theta) \sin(2\alpha) = -\mu J \cos(2\theta) \frac{u_x}{1 + u_x^2}. \quad (46)$$

Note that the surface current is downhill for θ less than the critical angle $\theta_c = \pi/4$ but is uphill for $\theta > \theta_c$. This shows very clearly that a flat initial surface is stable for $\theta < \theta_c$ and is unstable for $\theta > \theta_c$.

The total current is zero on a surface that has a selected slope. Equation (46) shows that there are no nonzero selected slopes in the case of the CV model except for $\theta = \theta_c = \pi/4$. For that angle, the total current vanishes for all slopes u_x and so there are no selected slopes in that case either. The CV model, however, is anomalous because $j(\theta_{\text{loc}})$ is an even function about the critical angle $\theta_{\text{loc}} = \pi/4$.

As an example that shows that there can be nonzero selected slopes for $\theta > \theta_c$ in the dual-beam problem, consider
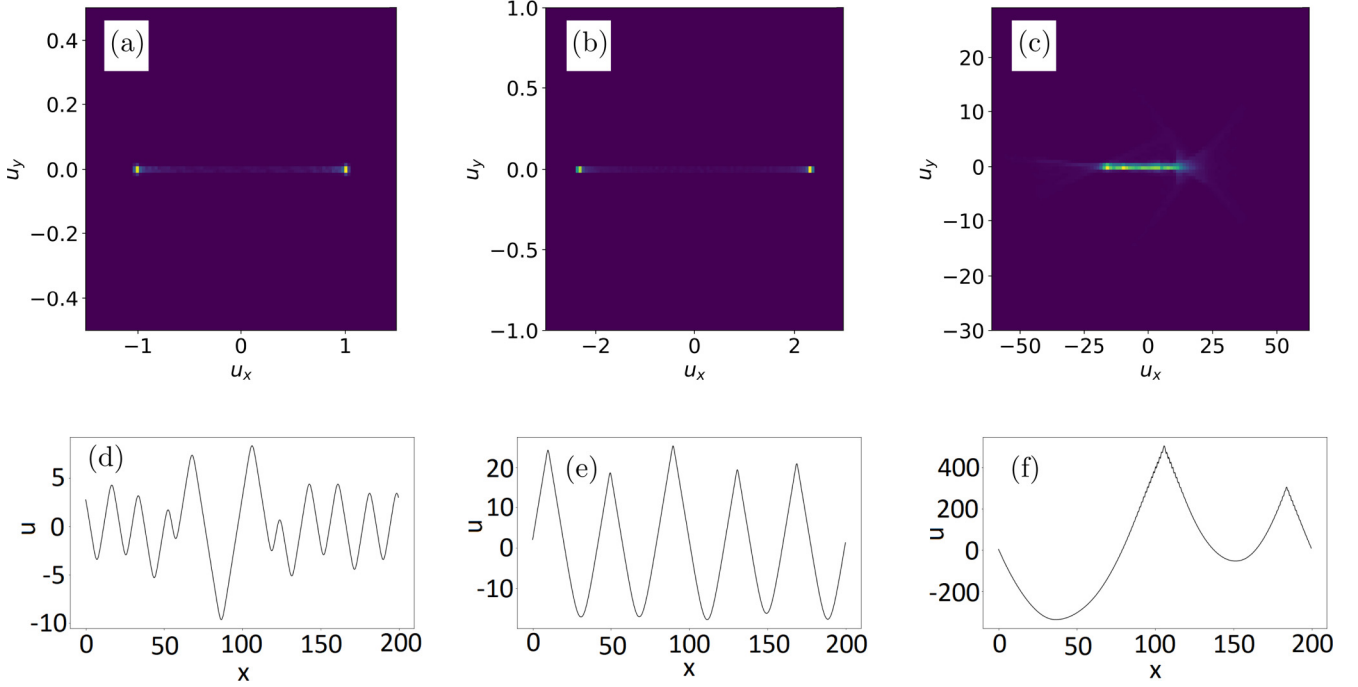
FIG. 2. (a)–(c) Slope distributions for the surfaces shown in Figs. 1(c), 1(f), and 1(i). (d)–(f) Cuts through the surfaces shown in Figs. 1(c), 1(f), and 1(i) taken at $y = 0$.

a different model of the surface current. In the CV model, every incident ion displaces an average mass proportional to $\sin \theta_{\text{loc}}$. Some ions, however, are elastically reflected from the solid surface and so displace no mass. Reflection of ions is particularly important at high angles of incidence. To make an easily analyzed model that takes the effect of ion reflection into account in a crude way, we will take the average displaced mass per ion to be proportional to $\sin \theta_{\text{loc}} \cos \theta_{\text{loc}}$. In this case, $j(\theta_{\text{loc}}) = \nu J \cos^2 \theta_{\text{loc}} \sin \theta_{\text{loc}}$, where ν is a positive constant of proportionality. The critical angle θ_c is the angle where $j(\theta_{\text{loc}})$ attains its maximum value, $\sin^{-1}(1/\sqrt{3}) \cong 35.26°$. $j(\theta_{\text{loc}})$ is not an even function about this angle. The total current for diametrically opposed beams is

$$j_{\text{tot}} = -\tfrac{1}{4}\nu J[\cos \theta \sin \theta + \cos(3\theta) \sin(3\alpha)]. \quad (47)$$

For $\theta \leqslant \theta_c$, this is zero only for $\alpha = 0$. For $\theta > \theta_c$, however, j_{tot} also vanishes for the nonzero tilt angles α given by $\sin^2 \alpha = \sec(3\theta)(1 - 3 \sin^2 \theta)$.

The EOM for the CV model with dual beams is $u_t = -\Omega \partial_x j_{\text{tot}}$, where j_{tot} is given by Eq. (46). Thus, to sixth order in ϵ,

$$\epsilon^4 U_T = -2\Omega \mu J \epsilon^4 \left(U_{XX} - \epsilon^2 \partial_X U_X^3\right). \quad (48)$$

To order ϵ^4, therefore, there is no term proportional to $\partial_X U_X^3$. Comparing this with Eq. (36), we see that for the CV model, $\gamma_3 = 0$ and hence $c = 0$. As a consequence, for the anomalous special case in which the slope dependence of the surface current is given correctly by the CV model, the 1D EOM is the CKS equation and there are no nonzero selected slopes.

VI. THE SCALING ANSATZ IS INVALID FOR A SINGLE INCIDENT BEAM

Consider the EOM (28) for a single incident beam with ion flux J. Since $C_{11} = -A_{11}\epsilon^2$,

$$J^{-1}U_T = -A_{11}U_{XX} + \epsilon^{-1}C_{111}U_{XXX} + C_{1111}U_{XXXX} \\ + C_{22}U_{YY} + \mu \partial_X^2 U_X^2 + \epsilon^{-1}\gamma_2 \partial_X U_X^2 + \gamma_3 \partial_X U_X^3.$$

$$(49)$$

Equation (49) does not have a well-defined $\epsilon \to 0$ limit unless $C_{111} = \gamma_2 = 0$. This means that the scaling ansatz given by Eqs. (6) and (7) is not appropriate for the case of a single incident beam unless both C_{111} and γ_2 happen to be zero at the critical angle. This, of course, is highly unlikely.

To get a sense of the source of the difficulties that arise when there is a single obliquely incident beam, let us suppose that the EOM were in fact given by Eq. (28), or, equivalently, Eq. (29). For simplicity, we will restrict our attention to the 1D case in which $u_y = 0$. The most serious problem stems from the presence of the term proportional to $\partial_x u_x^2$, and so let us suppose that its coefficient γ_2 is nonzero. To simplify the notation, earlier we set $a = J C_{11}$, $B = -J C_{1111}$, $c = J\gamma_3$, and $\beta = J\rho$. In addition, we define $\alpha \equiv J C_{111}$ and $b \equiv J\gamma_2$. Equation (29) becomes

$$u_t = \partial_x\left(au_x + bu_x^2 + cu_x^3\right) - Bu_{xxxx} + \alpha u_{xxx} + \beta \partial_x^2 u_x^2. \quad (50)$$

Recall that a is positive for $\theta < \theta_c$, is zero for $\theta = \theta_c$, and is positive for $\theta > \theta_c$. For simplicity, we will take the remaining coefficients in Eq. (29) to be constants that are independent of θ. For the problem to be well defined, c must be non-negative and B must be positive, and so we assume that this is the case, as we did previously for the dual-beam problem. We have

assumed that $\gamma_2 \neq 0$ and hence b is nonzero. In fact, we may take b to be positive without loss of generality because if it is not, we replace u by $-u$ in Eq. (50).

We will consider the special case in which $\alpha = \beta = 0$ to begin. To gain insight into the behavior of the surface, we study the resulting equation

$$u_t = \partial_x\left(au_x + bu_x^2 + cu_x^3\right) - Bu_{xxxx} \tag{51}$$

on a large but finite interval $0 \leqslant x \leqslant L$ and apply periodic boundary conditions. We also introduce the effective free energy

$$F \equiv \int_0^L \left[\frac{1}{2}Bu_{xx}^2 + f(u_x)\right]dx, \tag{52}$$

where

$$f(u_x) \equiv \tfrac{1}{2}au_x^2 + \tfrac{1}{3}bu_x^3 + \tfrac{1}{4}cu_x^4 \tag{53}$$

will be referred to as the effective potential. Equation (51) can be written

$$u_t = -\frac{\delta F}{\delta u}. \tag{54}$$

Equation (54) implies that $dF/dt \leqslant 0$; i.e., the effective free energy can never increase. The dynamics therefore tends to minimize the value of F.

Differentiating Eq. (51) with respect to x and again setting $\phi = u_x$, we obtain

$$\phi_t = \partial_x^2(a\phi + b\phi^2 + c\phi^3 - B\phi_{xx}). \tag{55}$$

The initial state of interest is a nominally flat surface, and so we take $\phi(x, 0)$ to be low-amplitude spatial white noise. Equation (55) with this initial condition is the CH equation for an off-critical quench [38]. The behavior of the solutions to this problem are well known and so we will simply summarize their properties here. For $a > a_c = 2b^2/(9c)$, the state $\phi = 0$ is stable. Thus, for incidence angles θ sufficiently far below θ_c, the surface smooths. In the coexistence region $0 < a < a_c$, on the other hand, there is a local minimum in the potential $f(\phi)$ at $\phi = 0$. The global minimum in the potential is at $\phi = \phi_* \equiv -(b + \sqrt{b^2 - 4ac})/2c < 0$. The state $\phi = 0$ is therefore metastable. Noise in the initial condition or shot noise in the ion beam will lead to nucleation and growth of regions with nonzero slopes ϕ_1 and ϕ_2 which satisfy $\phi_* < \phi_1 < 0$ and $\phi_2 > 0$. The surface slope varies smoothly in interfacial regions between adjacent intervals in which the slope is very nearly constant. The width of these interfacial regions depends on B. The precise values of the slopes ϕ_1 and ϕ_2 can be determined using the requirement that the line joining the points $(\phi_1, f(\phi_1))$ and $(\phi_2, f(\phi_2))$ must be tangent to the curve $f = f(\phi)$ at these two points. Finally, for $a \leqslant 0$, the state $\phi = 0$ is unstable and spinodal decomposition occurs. At long times, regions in which the slope is nearly equal to $(-b \pm \sqrt{b^2 - 4ac})/2c$ develop. Once again, adjacent intervals with differing, nearly constant slopes are separated by interfacial regions in which the slope varies smoothly.

The upshot of this discussion is that whether $0 < a < a_c$ or $a < 0$, at long times there will be regions in which the slope is nearly equal to a nonzero value that is not small. We began our derivation of the single-beam EOM, however, by assuming that Eqs. (6) and (7) apply. These equations imply

that u_x is proportional to $\epsilon = (\theta - \theta_c)^{1/2} \ll 1$ for θ just above the critical angle θ_c, i.e., for a that is small and negative. In contrast, our analysis of Eq. (51) shows that for θ close to θ_c, there will be regions in which the surface slope is of order 1 at long times. Thus, the small slope approximation inherent in the scaling ansatz given by Eqs. (6) and (7) is not valid if b is nonzero.

If there are diametrically opposed beams, b is zero and Eq. (55) becomes the CH equation for a critical quench. The flat surface is stable for $a > 0$, or, equivalently, for $\theta < \theta_c$. For θ just above θ_c (i.e., for small, negative a), spinodal decomposition occurs. Regions in which the surface slope is very nearly equal to $\pm\sqrt{|a|/c}$ develop at long times. Since $a \propto \epsilon^2$, these slopes are of order ϵ. This is consistent with the scaling ansatz.

So far, we have considered the special case of Eq. (50) in which $\alpha = \beta = 0$. A second special case of Eq. (50) in which b is nonzero has already been studied [44]. In this case, $c = 0$ but β is nonzero and α is arbitrary. It was shown analytically that for small, negative a (i.e., for $\epsilon \to 0$), slopes of order unity develop on the surface as time passes, and this was confirmed by simulations. Thus, in this case as well, the surface slope does not remain small and the scaling ansatz given by Eqs. (6) and (7) is invalid.

The discussion given in this section strongly suggests that if a single ion beam with $\theta \geqslant \theta_c$ is incident on the sample, the surface slope is not small everywhere at long times. If this is indeed the case, the surface current $\boldsymbol{j}$ would be needed for arbitrary local angles of incidence θ_{loc} before a full theory could be constructed. In the CV model [16], it is assumed that $\boldsymbol{j}$ points in the projected ion beam direction and that its magnitude is proportional to $\sin\theta_{loc}\cos\theta_{loc}$ for arbitrary θ_{loc}. However, this cannot be exactly correct because the CV model gives $\theta_c = 45°$ and this disagrees with experiment [12,15]. In addition, as already noted, molecular dynamics simulations show that $\boldsymbol{j}$ depends on the surface curvature, but it does not in the CV model [20]. Further progress on the single-beam problem in the low-energy regime may become possible once the dependence of $\boldsymbol{j}$ on θ_{loc} and the surface curvature has been studied in detail using atomistic simulations.

VII. DISCUSSION

As we have seen, the case in which diametrically opposed beams are simultaneously incident on the solid surface is much simpler than the single-beam case because in the former case, the EOM must be invariant under the transformation $x \to -x$. We obtained the EOM for diametrically opposed beams [Eq. (1)] by expanding Eq. (5) to order ϵ^4. If we instead expanded to order ϵ^6, we would recover Eq. (1), but with correction terms of order ϵ^2 appended to its right-hand side. Examples of terms of this kind are u_{xxyy}, $\partial_x^2 u_y^2$, $\partial_y^2 u_x^2$, and $\partial_x(u_x u_y^2)$. Close to threshold, ϵ is small and the correction terms can safely be neglected. However, as θ is increased, the correction terms gain in importance and the dynamical behavior of the surface would change. If θ is increased still further, the sign of the coefficient D in Eq. (1) could change at a second critical angle $\theta_{c,2}$. In this case, there would be an instability if the y direction for $\theta > \theta_{c,2}$ and it would be

necessary to include a term proportional to u_{yyyy} in the EOM [45].

We assumed that when a broad beam is incident on the surface, the ion flux is low enough that essentially all ion-induced motion near a point of ion impact, **P**, has ceased before another ion strikes the surface in the immediate vicinity of **P**. A hydrodynamic theory that applies when the ion energy is low enough that sputtering is negligible has been developed by Muñoz-García and co-workers [46]. This theory applies in the high-flux regime in which a whole layer at the surface of the target is mobilized by the ion impacts and behaves like a highly viscous fluid.

Equations that are related to our EOM (1) have been encountered in other physical contexts. When GaAs is maintained at a temperature in excess of its recrystallization temperature and is bombarded with a normally incident Ar$^+$ beam, highly ordered ripples form [14,47,48]. Ou *et al.* [47] have modeled time evolution of the GaAs surface using a variant of Eq. (1) in which the anisotropic terms $-Bu_{xxxx}$ and $\beta \partial_x^2 u_x^2$ are replaced by their isotropic counterparts $-B\nabla^2\nabla^2 u$ and $\beta\nabla^2(\nabla u)^2$. The term Du_{yy} in the EOM (1) suppresses variations of the surface height in the transverse direction, and so the differences in the time evolution produced by Eq. (1) and the equation studied by Ou *et al.* are expected to be modest.

Equations of motion that describe the instability of a growing crystal surface and that include the ES and CKS nonlinearities have been studied by Golubović and co-workers [33]. Our EOM (1) is a special case of the EOM they used to model the growth of a (110) surface [49–52], although they did not analyze the case $D > 0$ in which there is no instability in the transverse direction [53].

VIII. CONCLUSIONS

In this paper, we studied the behavior of a solid surface that is bombarded with two diametrically opposed, obliquely incident ion beams in the regime in which the ion energy is low enough that sputtering is negligible. For angles of incidence θ just above the threshold angle for ripple formation, θ_c, we carried out a systematic expansion in powers of the small parameter $\epsilon \equiv (\theta - \theta_c)^{1/2}$ and retained all terms up to fourth order in ϵ. We found that close to threshold and at sufficiently long times, the surface is governed by an anisotropic Cahn-Hilliard equation with an additional nonlinear term that breaks the up-down symmetry, Eq. (1).

Numerical integrations of Eq. (1) show that dual-beam ion bombardment in the low-energy regime leads to the formation of faceted parallel-mode ripples with a very low density of dislocations. These ripples are much more highly ordered than the ripples that usually result from ion bombardment of a solid surface. However, because the ripple wavelength varies in the longitudinal direction, the order is not perfect. This suggests that although the ripples have the sawtooth form that is needed for a blazed diffraction grating, they are not sufficiently regular for the grating to have a high efficiency.

We used a generalized crater function formalism to derive the EOM (1). The dependence of the crater function on spatial derivatives of the surface height of arbitrarily high order was taken into account. In addition, terms of all orders in the surface height u were retained in our derivation. (Close to the threshold for pattern formation, however, only terms of third order in u appear in the EOM to lowest nontrivial order in ϵ.) A by-product of our derivation of the EOM is expressions that relate the coefficients in the EOM to moments of the crater function. These expressions could be used to obtain estimates of the coefficients in the EOM from input produced by atomistic simulations. These estimates would include only the short-time or "prompt" effects of an ion impact that occur within picoseconds after the arrival of the ion, however. The contributions to these coefficients from slow processes like ion-induced viscous flow would have to be inferred from experiment or be computed by other means, as in past work [54].

Close to threshold, the surface slope remains small when diametrically opposed beams are incident on a surface that is initially flat. In contrast, our work strongly suggests that when a surface is bombarded with a single obliquely incident ion beam in the low-energy, no-sputtering regime, the surface slope does not remain small as the ripple amplitude grows. We therefore anticipate that developing a rigorous theory for the single-beam problem will be considerably more difficult than it was for the dual-beam problem.

ACKNOWLEDGMENTS

[1] For a review, see J. Muñoz-García, L. Vázquez, M. Castro, R. Gago, A. Redondo-Cubero, A. Moreno-Barrado, and R. Cuerno, Mater. Sci. Eng. R. **86**, 1 (2014).

[2] R. M. Bradley and J. M. E. Harper, J. Vac. Sci. Technol. A **6**, 2390 (1988).

[3] S. Facsko, T. Dekorsy, C. Koerdt, C. Trappe, H. Kurz, A. Vogt, and H. L. Hartnagel, Science **285**, 1551 (1999).

[4] F. Frost, A. Schindler, and F. Bigl, Phys. Rev. Lett. **85**, 4116 (2000).

[5] Q. Wei, X. Zhou, B. Joshi, Y. Chen, K.-D. Li, Q. Wei, K. Sun, and L. Wang, Adv. Mater. **21**, 2865 (2009).

[6] M. Fritzsche, A. Muecklich, and S. Facsko, Appl. Phys. Lett. **100**, 223108 (2012).

[7] L. Bischoff, W. Pilz, and B. Schmidt, Appl. Phys. A **104**, 1153 (2011).

[8] L. Bischoff, K.-H. Heinig, B. Schmidt, S. Facsko, and W. Pilz, Nucl. Instrum. Methods Phys. Res. Sect. B **272**, 198 (2012).

[9] R. M. Bradley and P. D. Shipman, Phys. Rev. Lett. **105**, 145501 (2010).

[10] P. D. Shipman and R. M. Bradley, Phys. Rev. B **84**, 085420 (2011).

[11] R. M. Bradley and P. D. Shipman, Appl. Surf. Sci. **258**, 4161 (2012).

[12] A. Metya and D. Ghose, Appl. Phys. Lett. **103**, 161602 (2013).

[13] D. Chowdhury, D. Ghose, and S. A. Mollick, Vacuum **107**, 23 (2014).

[14] D. Chowdhury, D. Ghose, S. A. Mollick, B. Satpati, and S. R. Bhattacharyya, Phys. Status Solidi B **252**, 811 (2015).

[15] A. Lopez-Cazalilla, D. Chowdhury, A. Ilinov, S. Mondal, P. Barman, S. R. Bhattacharyya, D. Ghose, F. Djurabekova, K. Nordlund, and S. Norris, J. Appl. Phys. **123**, 235108 (2018).

[16] G. Carter and V. Vishnyakov, Phys. Rev. B **54**, 17647 (1996).

[17] M. Moseler, P. Gumbsch, C. Casiraghi, A. C. Ferrari, and J. Robertson, Science **309**, 1545 (2005).

[18] B. Davidovitch, M. J. Aziz, and M. P. Brenner, Phys. Rev. B **76**, 205420 (2007).

[19] H. Hofsäss and O. Bobes, Appl. Phys. Rev. **6**, 021307 (2019).

[20] K. Nordlund (private communication).

[21] The effect that implantation of nonvolatile ions has on the surface dynamics is studied by R. M. Bradley and H. Hofsäss, J. Appl. Phys. **120**, 074302 (2016); H. Hofsäss, K. Zhang, and O. Bobes, *ibid.* **120**, 135308 (2016).

[22] R. Cuerno and A.-L. Barabási, Phys. Rev. Lett. **74**, 4746 (1995).

[23] M. A. Makeev, R. Cuerno, and A.-L. Barabási, Nucl. Instrum. Methods Phys. Res. Sect. B **197**, 185 (2002).

[24] R. M. Bradley, Phys. Rev. E **102**, 012807 (2020).

[25] S. A. Norris, M. P. Brenner, and M. J. Aziz, J. Phys. Condens. Matter **21**, 224017 (2009).

[26] M. P. Harrison and R. M. Bradley, Phys. Rev. B **89**, 245401 (2014).

[27] M. Joe, C. Choi, B. Kahng, and J.-S. Kim, Appl. Phys. Lett. **91**, 233115 (2007).

[28] M. Joe, J.-H. Kim, C. Choi, B. Kahng, and J.-S. Kim, J. Phys.: Condens. Matter **21**, 224011 (2009).

[29] J.-H. Kim, M. Joe, S.-P. Kim, N.-B. Ha, K.-R. Lee, B. Kahng, and J.-S. Kim, Phys. Rev. B **79**, 205403 (2009).

[30] M. P. Harrison and R. M. Bradley, J. Phys.: Condens. Matt. **27**, 295301 (2015).

[31] A more complete review of the literature on the effects of bombardment with multiple ion beams and on the effects of discrete sample rotations during ion bombardment with a single beam may be found in Ref. [30].

[32] C. C. Umbach, R. L. Headrick, and K.-C. Chang, Phys. Rev. Lett. **87**, 246104 (2001).

[33] L. Golubović, A. Levandovsky, and D. Moldovan, E. Asian J. Appl. Math. **1**, 297 (2011).

[34] J. Villain, J. Phys. I (France) **1**, 19 (1991).

[35] M. Castro, R. Cuerno, L. Vazquez, and R. Gago, Phys. Rev. Lett. **94**, 016102 (2005).

[36] J. Muñoz-García, M. Castro, and R. Cuerno, Phys. Rev. Lett. **96**, 086101 (2006).

[37] J. Muñoz-García, R. Cuerno, and M. Castro, Phys. Rev. B **78**, 205408 (2008).

[38] R. C. Desai and R. Kapral, *Dynamics of Self-Organized and Self-Assembled Structures* (Cambridge University Press, Cambridge, UK, 2009).

[39] M. Raible, S. J. Linz, and P. Hänggi, Phys. Rev. E **62**, 1691 (2000).

[40] T. Frisch and A. Verga, Phys. Rev. Lett. **96**, 166104 (2006).

[41] K. M. Loew and R. M. Bradley, Phys. Rev. E **100**, 012801 (2019).

[42] For the case in which $\sin\psi = 1$, a term $0.1u_{xxxxxx}$ was added to the right-hand side of Eq. (41) to prevent the onset of a numerical instability as the cusps became sharper.

[43] F. Liu and H. Metiu, Phys. Rev. B **48**, 5808 (1993).

[44] M. P. Gelfand and R. M. Bradley, Phys. Lett. A **379**, 199 (2015).

[45] If $D < 0$ and $D < a$, the ripples that form are so-called perpendicular-mode ripples (ripples with their wave vector lying in the y direction). Because perpendicular-mode ripples have frequently been observed in experiments, there is experimental evidence for the existence of a second critical angle where D becomes negative for at least some choices of target material and ion beam.

[46] J. Muñoz-García, R. Cuerno, and M. Castro, Phys. Rev. B **100**, 205421 (2019).

[47] X. Ou, K.-H. Heinig, R. Hübner, J. Grenzer, X. Wang, M. Helm, J. Fassbender, and S. Facsko, Nanoscale **7**, 18928 (2015).

[48] D. Chowdhury and D. Ghose, Vacuum **129**, 122 (2016).

[49] L. Golubović, A. Levandovsky, and D. Moldovan, Phys. Rev. Lett. **89**, 266104 (2002).

[50] A. Levandovsky, L. Golubović, and D. Moldovan, Phys. Rev. E **74**, 061601 (2006).

[51] A. Levandovsky and L. Golubović, Phys. Rev. E **76**, 041605 (2007).

[52] L. Golubović and A. Levandovsky, Phys. Rev. E **77**, 051606 (2008).

[53] Golubović and co-workers also claimed that their work applies to ion erosion of crystal surfaces. This is questionable at best, since they did not specify the angle of incidence of the ion beam and did not consider the dependence of the sputter yield on the angle of incidence or the surface curvature.

[54] S. A. Norris, J. Samela, L. Bukonte, M. Backman, F. Djurabekova, K. Nordlund, C. S. Madi, M. P. Brenner, and M. J. Aziz, Nat. Commun. **2**, 276 (2011).